1	A Novel Cylindrical Overlap-and-Fling Mechanism Used by Sea Butterflies
2	Ferhat Karakas <sup>1</sup> , Amy E. Maas <sup>2</sup> and David W. Murphy <sup>1</sup>
3 4 5	<sup>1</sup> Department of Mechanical Engineering, University of South Florida, Tampa, FL 33620 <sup>2</sup> Bermuda Institute of Ocean Sciences, St. George's GE01, Bermuda
6 7	Corresponding author contact: davidmurphy@usf.edu
8	Abstract
9	The clap-and-fling mechanism is a well-studied, unsteady lift generation mechanism widely
10	used by flying insects and is considered obligatory for tiny insects flying at low to
11	intermediate Re. However, some aquatic zooplankters including some pteropod (i.e. sea
12	butterfly) and heteropod species swimming at low to intermediate Re also use the clap-and-
13	fling mechanism. These marine snails have extremely flexible, actively deformed, muscular
14	wings which they flap reciprocally to create propulsive force, and these wings may enable
15	novel lift generation mechanisms not available to insects, which have less flexible, passively
16	deformed wings. Using high-speed stereophotogrammetry and micro-particle image
17	velocimetry, we describe a novel cylindrical overlap-and-fling mechanism used by the
18	pteropod species Cuvierina atlantica. In this maneuver, the pteropod's wingtips overlap at the
19	end of each half-stroke to sequentially form a downward-opening cone, a cylinder, and an
20	upward-opening cone. The transition from downward-opening cone to cylinder produces a
21	downward-directed jet at the trailing edges. Similarly, the transition from cylinder to upward-
22	opening cone produces downward flow into the gap between the wings, a leading edge vortex
23	ring, and a corresponding sharp increase in swimming speed. The ability of this pteropod
24	species to perform the cylindrical overlap-and-fling maneuver twice during each stroke is
25	enabled by its slender body and highly flexible wings. The cylindrical overlap-and-fling
26	mechanism observed here may inspire the design of new soft robotic aquatic vehicles
27	incorporating highly flexible propulsors to take advantage of this novel lift generation
28	technique.
29	KEY WORDS: Leading edge vortex, pteropod, PIV, soft robotics, flexible, insect flight
30	<b>Summary:</b> Enabled by its highly flexible wings, the swimming pteropod <i>C. atlantica</i>
31	generates thrust by using a novel cylindrical 'overlap-and-fling' maneuver twice during each
32	wingstroke.

**Running Title:** Swimming of the pteropod *C. atlantica* 

### Introduction

The aerodynamics of flapping flight by insects, birds, and other organisms is highly complex, and many unsteady lift-enhancing flow phenomena have been discovered (Weis-Fogh, 1973; Dickinson et al., 1999; Bomphrey et al., 2017). The best known of these is the clap-and-fling mechanism, originally described by Weis-Fogh (1973). The clap-and-fling mechanism is widely used by insects and seems to be obligatory in the smallest insects (Kolomenskiy et al., 2011; Sane, 2016; Cheng and Sun, 2018). In the clap-and-fling mechanism, the wings closely approach each other at the end of the recovery stroke (the clap phase) and force the flow in the gap between them downwards in a jet-like flow to enhance lift generation. The wings then rotate apart from each other about their trailing edges (the fling phase), creating a V-shaped gap into which air flows. In this way, insects overcome the starting Wagner effect, create a low pressure region between the wings, and create enhanced leading edge vortices.

The clap-and-fling mechanism has been widely studied since its discovery. Lighthill (1973) performed theoretical analysis with simplifying assumptions, showing how the clap-and-fling mechanism increases lift generation. Using a dynamically scaled laboratory model, Maxworthy (1979) visualized the leading edge vortices formed in the fling phase and found they comprise a large part of the force generated. Ellington (1984) reported variations of the clap-and-fling maneuver, including the near-clap-and-fling and the clap-and-peel, in various insect species. Lehmann et al. (2005) used dynamically scaled fruit fly wing models to find that the clap-and-fling mechanism enhanced the resultant force by 17%. Kolomenskiy et al. (2011) concluded from their theoretical and computational 2D model that viscosity enhances lift generation in the 'fling' as compared to the inviscid case. Computational fluid dynamics studies of the clap-and-fling mechanism have recently highlighted the importance of wing flexibility and porosity in overcoming the large forces needed for tiny insects to clap their wings together and fling them apart (Miller and Peskin, 2005; Miller and Peskin, 2009; Santhanakrishnan et al., 2014) and have shown that flexible wings can reduce the drag force generated during the fling by about 50% (Miller and Peskin, 2009).

Research by Satterlie et al (1985) and Borrell et al (2005) on the swimming of the shell-less marine snail *Clione limacina* and its congener *Clione antarctica* suggested that the clap-and-fling maneuver is not limited to aerial flight. Based on high speed filming of tethered organisms, Chang and Yen (2012) showed that the tiny (~2 mm) shelled pteropod *Limacina helicina* similarly uses a version of the clap-and-fling maneuver with its pair of

highly flexible, wing-like appendages (called parapodia) formed from a modified foot structure. Murphy et al (2016) used volumetric particle image velocimetry to measure the kinematics and flows generated by *L. helicina* performing its clap-and-fling mechanism, findings which were verified by Adhikari et al. (2016) in *Limacina helicina antarctica*. Similarly, Karakas et al. (2018) found that the heteropod *Atlanta selvagensis* performs a clap-and-fling maneuver using its one flexible appendage and its rigid, coiled shell. Here we report a novel variation of the clap-and-fling mechanism used by another sea butterfly species, *Cuvierina atlantica*, which we call a cylindrical overlap-and-fling.

### Materials and methods

## **Species and environment**

A variety of shelled pteropod species including *C. atlantica*, *Hyalocylis striata*, *Heliconoides inflatus*, and *Limacina bulimoides* were collected from offshore of Bermuda using a Reeve net with 150 µm mesh size and a specialized 20 l cod end. Specimens were collected during a nighttime cruise, kept in collected seawater, and brought back to a temperature-controlled chamber at the Bermuda Institute of Ocean Sciences (BIOS) in May 2017. The zooplankton were sorted and visually identified under a stereomicroscope and were then stored in filtered sea water at an *in situ* temperature of 21 °C. To ensure that specimens were healthy, experiments were conducted immediately upon return from the cruise and, since the pteropods did not live long after capture, experiments were completed within 36 hours of collection. This mixed assemblage of pteropod species was placed together in the experimental systems described below. At least two *C. atlantica* individuals were included in this assemblage, and these could be differentiated in the recordings based on shell length.

# 3D Kinematics setup

A photogrammetry system comprising two synchronized high-speed monochrome Edgertronic cameras (Sanstreak Corp., San Jose, CA, USA) was used to measure the three-dimensional swimming kinematics of the pteropods at high magnification. The cameras, lights, and aquarium were mounted on optical rails and a breadboard to rigidly support the system. The two cameras were arranged perpendicular to each other and were equipped with 200 mm Nikon macro lenses with apertures set to f/32 to maximize the depth of the field (~12 mm). Both cameras filmed at 600 Hz with a resolution of 1024×912 pixels and viewed a

glass aquarium with  $30\times30\times30$  mm<sup>3</sup> (W × D × H) inner dimensions and 2.5 mm wall thickness, which was filled with 0.2 µm filtered seawater collected with the pteropods to a depth of 28 mm. The field of view of each camera was at least 10 mm above the tank bottom such that only actively swimming pteropods were recorded. The focal planes of the cameras were set to the middle of the aquarium so that only freely swimming pteropods not interacting with the walls would be recorded. The spatial resolution of the cameras was 14.3 μm pixel<sup>-1</sup>. Collimated backlighting for each camera was provided by an LED fiber optic illuminator with a dual arm gooseneck (Dolan-Jenner Industries, Lawrence, MA, USA). The camera system was spatially calibrated prior to the experiments using the direct linear transform technique (Abdel-Aziz and Karara, 1971; Hedrick, 2008). Briefly, a scaled microscope slide held vertically and oriented 45° to both cameras was positioned at 25 predefined locations within the common field of view within the filled aquarium using a microtranslator (PT3/M, Thorlabs, Newton, New Jersey, USA). Three points on the slide imaged at these 25 locations provided 75 calibration points covering the measurement volume. These points provided the calibration coefficients mapping the 2D camera coordinates into the 3D world coordinates using DLTdv5 (Hedrick, 2008). Up to approximately 10 pteropods of diverse sizes and species were selected for the experiments and were carefully transferred to the test aquarium. Little interference was observed between swimming animals since swimming bouts were intermittent and alternated with periods of lying on the tank bottom. The camera system was manually triggered when a pteropod swam into the field of view common to both cameras. Four videos of C. atlantica representing two different individuals were collected. However, because of the high magnification, parts of the pteropod were often outside the field of view of one camera for some part of these videos. Thus, a 0.43 s segment from one recording event in which the animal swam upwards through the field of view and in which both wings were fully visible for almost two complete wing strokes was chosen for further analysis. As shown in Fig. 1, ten different points on the pteropod were manually tracked in each frame using DLTdv5 in order to quantify the pteropod wing and body kinematics (Hedrick, 2008). Kinematics data from one video in which the pteropod swam upwards through the field of view are presented in the Results.

### PIV setup

99

100

101

102

103

104

105

106

107

108

109

110

111

112

113

114

115

116

117

118

119

120

121122

123

124

125

126

127

128

129

130

131

Brightfield back-illuminated 2D micro particle image velocimetry ( $\mu$ PIV) was applied to quantify the flow structures and velocity fields around the freely swimming pteropods (Gemmell et al., 2014). In this system, a 2× extra-long working distance (ELWD)

microscopic objective (#46-142, Mitutoyo) with an image-generating tube lens (#58-520, Edmund Optics) provided a depth of field of 91 µm, resulting in a measurement plane width (MPW) of approximately 250 µm (Koutsiaris, 2012). The advantage of this approach is its ability to provide a narrow measurement plane width without the use of a laser. A high-speed camera (Phantom VEO 640S) recorded at 1400 Hz with a spatial resolution of 2560×1600 pixels. The field of view was 12.43×7.77 mm<sup>2</sup> (vertical × horizontal) and was vertically and horizontally centered within the tank in order to minimize wall and free surface effects. The test tank was seeded with 2-3 µm mean diameter algae (Nannochloropsis oculata), which work well as tracking particles because they are natural food items for pteropods (Thabet et al., 2015) and because no light scattering by the particles is required. The test section was illuminated with a telecentric backlight illuminator (#62-760, Edmund Optics). Similar to the kinematics experiments, multiple pteropods were placed in the aquarium simultaneously. Recordings were manually triggered when an animal swam through the focal plane. Six videos of C. atlantica were recorded, but only in one video did this species perform a complete stroke cycle while well positioned in the focal plane. This video, which recorded the same individual for which kinematics data were analyzed, was chosen for further flow analysis. Image processing was applied to the raw µPIV images to invert the images, apply Gaussian filtering to remove out-of-focus particles, and algorithmically mask animals using local intensity values. Velocity fields were calculated by applying multi-pass crosscorrelation using a 50% overlap, beginning with a 64×64 window size in the first pass and decreasing to 32×32 window sizes in subsequent passes. Erroneous vectors were removed by the universal outlier detection method. Particle seeding density was high, with about 20 particles distributed in each 64×64 interrogation window. The resulting vector fields comprised 160×100 vectors with a vector grid spacing of 0.0766 mm.

## **Results**

132

133

134

135

136

137

138

139

140

141

142

143

144

145

146

147

148

149

150

151

152

153

154

155

156

157

158

159

160

161

162

163

164

Fig. 1 shows a three-dimensional model of the shelled pteropod C. atlantica with the tracked points labeled, including three points on the body (c-e), the wingtips (a-b), the leading edges (f and h) and trailing edges (g and i) of the right and left wing chords, and a point on the top edge of the shell (j, coinciding with the origin of the body-centered coordinate system). A global (XYZ) coordinate system and a body-centered <math>(X'Y'Z') coordinate system, which translates and rotates with the animal, also are defined in Fig. 1. As measured from the 3D coordinates taken from the processed kinematics videos, the adult pteropod has a body length of  $l_b=9\pm0.03$  mm (a mean  $\pm$  standard deviation value measured

from point c to d over 116.7 ms), a wingspan of  $l_s$ =9.4 ± 0.1 mm (a mean ± standard deviation value measured between points a and b at the three time points in the recording when the wings are fully outstretched, as in Fig. 1A), and a chord length of  $c=3.0\pm0.27$  mm (a mean  $\pm$  standard deviation value measured between points f and g over 408.3 ms). It is important to note that these mean and standard deviation values represent multiple measurements of the same animal taken at different time points within the same recording. The animal beats its wings at a mean frequency of f=5 Hz and has a mean swimming speed  $\bar{u}$ of 35 mm s<sup>-1</sup>. These animals thus swim in an intermediate Reynolds number regime in which both inertial and viscous forces are important. A body-based Reynolds number  $Re_b=\bar{u}l_b/\nu$ and chordwise Reynolds number  $Re_c = 2\varphi f l_f c/\nu$  are defined here, where  $l_f$  is the length of one wing,  $\varphi$  is wing stroke amplitude, and  $\nu$  is the kinematic viscosity of the sea water at 21 °C. Given that C. atlantica has a wing stroke amplitude of  $\varphi = 160^{\circ}$ , this pteropod species thus has a  $Re_b = 300$  and  $Re_c = 420$ , placing its  $Re_c$  in the same order of magnitude as that of fruit flies (Vogel, 1966). As shown in Fig. 1B, the animal's pitching angle  $\theta$  is defined as the angle between the Z and Z' axes. The wing bending angle  $\beta$  is defined for each wing using points on the wingtip, mid-wing chord, and body, as shown in Fig. 1C for the left wing.

Fig. 2 shows a model of C. atlantica which illustrates the motion of its wings as the animal performs an idealized cylindrical overlap-and-fling maneuver as well as simplified schematics comparing the cylindrical overlap-and-fling maneuver to the classic clap-and-fling maneuver used by insects. High speed visualization, wingtip and body kinematics, and the resulting flow fields throughout one wing stroke are then presented in order to illustrate the principle of the cylindrical overlap-and-fling mechanism and how it is used by C. atlantica. Thus, Fig. 3 shows the C. atlantica wing stroke cycle from two synchronized orthogonal high speed cameras (Movie 1). Due to the highly flexible nature of the wings, the outer edge of the right wing in both perspectives is highlighted in red for clarity. Fig. 4 shows the time history of the right and left wingtip positions (in the body-centered coordinate system), body angle  $\theta$ , instantaneous swimming speed U, and the wing bending angle  $\bar{\beta}$  averaged between the right and left wings. Fig. 5 shows flow fields recorded in a plane slightly offset from the pteropod's sagittal plane (Movie 2). The approximate location of this plane relative to the pteropod is shown in Fig. 2.

As shown in Fig. 2A and Fig. 3, at the beginning of the wingbeat cycle (t'=0), the right and left wings are highly bent along their respective spans, with  $\bar{\beta}$  up to 160° (Fig. 4B), and overlap each other to form a circular cylinder on the posterior side of the animal. This

wingtip overlap is reflected in the positive Y' position of the right wingtip and the negative Y' position of the left wingtip in Fig. 4B. As the power stroke commences (t' = 0.1), the wings separate from each other as the right and left wingtip Y' positions cross (Fig. 4B). As they expand from their cylindrical configuration,  $\bar{\beta}$  decreases (Fig. 4B), the X' wingtip positions slightly decrease (Fig. 4A), and the Z' positions increase (Fig. 4C) as the wings elevate and open away from the body simultaneously. As shown in Fig. 2B and Fig. 3, the leading edges of the wings open from their cylindrical shape more quickly than the trailing edges, thus transforming the cylinder into a conical shape with a larger opening on the top than on the bottom. The result of this fling part of the cylindrical overlap-and-fling maneuver is that a vortex ring seems to form on the wings' leading edges which feeds flow into the gap opening between the wings, a concept illustrated in Fig. 2A-C. For example, Fig. 5 shows a clockwise vortex developing on the right wing's leading edge at t' = 0.12 and strengthening as the wings further separate at t' = 0.15-0.19. This fling results in a strong downward flow adjacent to the animal's shell, with flow speeds reaching a maximum of 121 mm s<sup>-1</sup> at t' = 0.19. This maneuver coincides with a sharp increase in swimming speed from 10 mm s<sup>-1</sup> to 30 mm s<sup>-1</sup> as shown in Fig. 4D.

Subsequently, the X' wingtip positions continue to increase as the wing stroke continues toward the anterior side of the animal (Fig. 4A). By t' = 0.25 in Fig. 3, the wings are fully extended as the Y' wingtip coordinates reach their maximum negative and positive values for the right and left wings, respectively (Fig. 4B). The wing bending angle  $\bar{\beta}$  approaches zero and subsequently becomes negative as the fully extended wings cross to the anterior side of the animal (Fig. 4B). As shown in Fig. 5 at t' = 0.23, a strong clockwise vortex remains on the animal's posterior side and is transported downwards; no significant flow around the wing is seen at this time because the view is obstructed by the other wing and because the focal plane is near the root of the wing (Fig. 2C). As shown in Fig. 4D, this anterior wing flapping coincides with an increase in  $\theta$  as the top of the shell pitches posteriorly and with the local maximum swimming speed of 50 mm s<sup>-1</sup> at approximately t' = 0.26. The flow field at t' = 0.33 in Fig. 5 show a tip vortex on the right wing; it is likely that this vortex wraps around the animal to connect with the previously shed vortex on the animal's posterior side.

At t' = 0.4 in Fig. 3, the wings have almost finished their respective power strokes and have traveled to the anterior side of the animal, as shown by the Y' wingtip coordinates converging in Fig. 4B. Here the wingtips overlap, as shown by the crossing traces of the

wingtip Y' positions and form a cone. This cone initially has a wider diameter on the bottom than on the top but becomes cylindrical as the wings are pulled back towards the shell, as illustrated in Fig. 2D-F. The local minima in the X' wingtip positions at approximately t' = 0.5 in Fig. 4A also illustrate how the wings must bend to close into a cylinder. The resulting flow, a downward jet of fluid squeezed out from the cone between the wings, is shown at t' = 0.40 in Fig. 5. This jet has flow speeds of 78.5 mm s<sup>-1</sup>, feeds into the existing tip vortex, and rolls up to form what is likely a small vortex ring which travels downwards anterior to the animal. This concept is illustrated in Fig. 2D-F. The weaker flow speeds generated by this cylindrical overlap do not result in an increase in swimming speed as instead the animal continues to decelerate during this time period (Fig. 4D). The downward jet thus may serve to clear the previously generated vortex structures in preparation for the next half-stroke (Dickinson, 1996).

At t' = 0.53 in Fig. 3 and t' = 0.51 in Fig. 5, the pteropod has finished its power stroke and, with its wing bending angle (Fig. 4B) and swimming speed at a minimum, begins its recovery stroke. The pteropod thus performs a second fling maneuver similar to that performed during the power stroke. Specifically, the wings begin to unfold from their cylindrical configuration in which the wingtips overlap with each other, evidenced by increasing  $\bar{\beta}$  (Fig. 4B). This unfolding also is shown by the increase in the X' wingtip positions and crossing of the Y' wingtip traces in Fig. 4A and Fig. 4B, respectively. As the wings unfold, the leading edges open before the trailing edges, again transforming the cylinder into a cone, as shown in Fig. 2B and at t' = 0.66 in Fig. 3. This second fling maneuver again causes a vortex to form around the wing's leading edges and fluid to flow into the opening conical gap between the wings, resulting in a sharp increase in the pteropod's swimming speed (Fig. 4D). This downward flow between the wings is shown at t'= 0.64 in Fig. 5 and has a maximum speed of 94 mm s<sup>-1</sup>, slightly less than the maximum speed measured during the power stroke's fling. This vortex and downward flow continue to develop at t' = 0.70 in Fig. 5 as the pteropod continues with its recovery stroke (t' = 0.75 in Fig. 3). The body angle reaches its minimum ( $\theta = -7.4^{\circ}$ ) near the end of the recovery stroke and subsequently begins to increase, as shown in Fig. 4D. At the end of the recovery stroke (t'= 0.92 in Fig. 3), the swimming speed decreases to 15 mm s<sup>-1</sup> and the wings perform a second overlap maneuver as they fold together to form a cone which transforms into a cylinder. The wings are thus in position to perform the fling associated with the next power stroke.

### Discussion

The lift-enhancing clap-and-fling maneuver as used by most insects and some marine snails consists of the close apposition of largely flat wings (Ellington, 1984; Murphy et al., 2016; Karakas et al., 2018). Apposing and separating these flat wings in close proximity to each other during the clap and fling phases, respectively, requires a large amount of power, especially at Re < 10, though this drag-induced energetic expense is reduced somewhat by increased wing flexibility and porosity (Miller and Peskin, 2005; Miller and Peskin, 2009; Santhanakrishnan et al., 2014). In contrast, the pteropod species studied here uses its highly flexible wings to sequentially form a downward-opening cone, a cylinder, and an upwardopening cone at the end of each half stroke. We call this novel lift-enhancing technique the cylindrical overlap-and-fling. Though serving the same function as in insects, the geometrical configuration of the wings is dramatically different. This novel geometry allows this pteropod species to take advantage of the lift enhancement offered by the clap-and-fling maneuver without the necessity of wing apposition. The cylindrical overlap-and-fling maneuver may thus offer the possibility of avoiding the large drag associated with the classic 'planar' clapand-fling maneuver. However, the Reynolds number at which C. atlantica uses the overlapand-fling ( $Re_b = 300$  and  $Re_c = 420$ ) is somewhat larger than the Reynolds number at which most insects use the clap-and-fling. Indeed, the clap-and-fling maneuver is thought to be obligatory for tiny insects flying at Reynolds numbers of 100 or less. However, large insects also perform the clap-and-fling maneuver in high Re flight, especially to generate extra lift (e.g. Locusta migratoria in climbing and turning flight (Cooter and Baker, 1977), the butterfly Vanessa atalanta (Srygley and Thomas, 2002), and some other large insects carrying loads (Marden, 1987)). Indeed, Marden (1987) showed that use of clap-and-fling by various insects, small birds, and bats increases the lift per unit flight muscle mass by about 25% as compared to flight in the absence of the clap-and-fling maneuver, and Lehmann et al. (2005) measured a 17% increase in lift generation in a dynamically scaled *Drosophila* wing model ( $Re \sim 100-200$ ) which performs a near-clap-and-fling maneuver. It is likely that pteropods employing a version of the clap-and-fling at  $Re_c$ =5-35 (e.g. L. helicina; Murphy et al., 2016) and the overlap-and-fling at higher Re (e.g C. atlantica) enjoy similar lift augmentation. However, it is unknown whether the cylindrical overlap-and-fling maneuver is employed by smaller pteropod species or juvenile C. atlantica individuals swimming at Re characteristic of tiny insect flight. The need for such extreme and complex wing deformation may possibly limit use of the overlap-and-fling maneuver to somewhat larger wing sizes and larger Re.

264

265

266

267

268

269

270

271

272

273

274

275

276

277

278

279

280

281

282

283

284

285

286 287

288

289

290

291

292

293

294

295

A second significant difference in the ways that pteropods and insects use this type of clap-and-fling maneuver is that C. atlantica performs two complete overlap-and-fling maneuvers in each wing stroke while all insects studied to date and some other pteropod species (e.g. L. helicina) are only able to perform one. This ability in C. atlantica is enabled by its highly flexible wings which may bend 160° in both anterior and posterior directions and by the fact that its body and elongated shell, a more recent evolutionary shift in pteropod morphology as compared to spiraled shell pteropods (Peijnenburg et al. in review; Janssen and Peijnenburg, 2017), do not interfere with its wing motion. Insects, on the other hand, have relatively less flexible wings, and clapping at the end of the power stroke has not been reported, likely because the presence of their bodies prevents the wings from clapping at the end of the power stroke (Lighthill, 1973; Wootton, 1981; Cheng and Sun, 2017). Similarly, some other pteropod species, though they do have highly flexible wings, are prevented from clapping twice during each stroke because of the presence of their spiral shaped shell (Chang and Yen, 2012; Adhikari et al., 2016; Murphy et al., 2016). In contrast, enabled by its slender body and extremely large stroke angle, the atlantiid heteropod A. selvagensis performs a double clap-and-fling on each stroke without significant bending of its appendages (Karakas et al., 2018). The ability to use the clap-and-fling maneuver twice during each stroke was theoretically considered by Lighthill (1973) who hypothesized that this double use would create a circular vortex ring on each half-stroke in the animal's wake, thereby maximizing downward momentum per unit kinetic energy. Though volumetric velocity measurements are needed for confirmation, it seems likely that its large wing stroke amplitude and low wingbeat frequency enable C. atlantica to indeed create two independent vortex rings throughout each stroke cycle. The wake in this scenario would represent a real life case of Dickinson's (1996) idealized fish propelling itself via large amplitude pectoral fin strokes and thus creating a series of disconnected vortex loops in its wake. Indeed, the separation between the vortices created by the power and recovery strokes seen in Fig. 5 show that this is likely the case. Regardless of the wake structure, the additional lift provided by using the overlapand-fling mechanism twice during each stroke is beneficial in supporting the heavy shell of C. atlantica as it daily migrates at least 100 m upwards to the ocean surface to feed (Wormuth, 1981).

297

298

299

300

301

302

303

304

305

306

307

308

309

310

311

312

313

314

315

316

317

318

319

320

321

322

323

324

325

326

327

328

329

330

Another significant difference between pteropods' overlap-and-fling and insects' clap-and-fling is that *C. atlantica* actively bends its wings whereas the wings of insects are passively deformed depending on the aerodynamic load (Wootton, 1981; Wootton, 1990; Combes and Daniel, 2003a; Combes and Daniel, 2003b). Indeed, this pteropod is able to bend

its wings along the spanwise direction to such an extent that its wingtips overlap at the end of each half stroke. The active flexibility of pteropod appendages is due to their unique morphology and wing structure. Pteropod wings are modified from the molluscan foot without any rigid support (Borrell et al., 2005), and these organisms have hydrostatic skeletons which are supported by fluid pressure (Szymik and Satterlie, 2017). Further, the wings of pteropods have layers of parallel muscles oriented at different angles across the wing (Satterlie et al., 1985). This unique wing structure enables active spanwise wing bending and high flexibility, with wing bending angle amplitudes up to 160° in C. atlantica (Fig. 4B). In contrast, insects have exoskeletons and their wings, which are actuated at their roots, have a complex network of veins with connecting membranes to support the forces on the wings (Wootton, 1981). Active spanwise wing deformation is thus absent, and passive wing deformation in insects is mostly limited to an amplitude of less than 40 degrees (Lucas et al., 2014). Wing flexibility in insects has been shown to be beneficial with higher energetic efficiency and aerodynamic performance (Vanella et al., 2009; Colin et al., 2012; Kodali et al., 2017; Wong and Rival, 2017). Wong and Rival (2017) showed that passive spanwise bending of 30-40° stabilizes the leading edge vortex (LEV), thus providing augmented lift for an extended period of time. In contrast, these researchers found that active spanwise bending of the same magnitude generates a much stronger yet less stable LEV than that generated either with passive bending or in the absence of bending, thus generating higher levels of instantaneous lift. Cuvierina atlantica utilizes passive spanwise bending as the wings separate after each overlap-and-fling. The mid-span of each convex-shaped wing thus leads during the first part of each half-stroke. Midway through each stroke (i.e. leading into the overlap phase), the convexity of the wing reverses as the tip begins to lead, thus changing into an active spanwise bending configuration. This mechanism may provide an effective way to actively control the strength and stability of the LEV over the wing stroke and thus to manipulate the lift generation.

331

332

333

334

335

336

337

338

339

340

341

342

343

344

345

346

347

348

349

350

351

352

353

354

355

356

357

358

359

360

361

362

363

364

In addition to controlling spanwise bending, pteropods are also able to actively control chordwise bending owing to their fluid-filled wings which have infinite degrees of freedom in motion. This chordwise deformation is actively controlled by the fluid pressure and by muscle fibers in the wing, with the control system based on complex feedback from the surrounding flow conditions (Szymik and Satterlie, 2017). Active control over chordwise flexibility likely enables *C. atlantica* to perform the overlap-and-fling maneuver as it moves its overlapping wings from a cylindrical configuration to a conical configuration. Chordwise wing flexibility similarly enables insects and micro aerial vehicles to generate greater lift-to-

drag ratios when performing the clap-and-fling or clap-and-peel maneuver. For example, Miller and Peskin (2009) numerically showed a 50% decrease in peak drag in the fling due to wing flexibility and an increase in lift force in some cases. Similarly, flow and force measurements on a pair of flexible model wings performing clap-and-peel showed relatively higher force generation as compared to rigid wings (Percin et al., 2017).

365

366

367

368

369

370

371

372

373

374

375

376

377

378

379

380

381

382

383

384

385

386

387

388

389

390

391

392

393

394

395

396

397

Though all pteropod species swim by flapping a pair of structurally similar highly flexible parapodia, swimming kinematics may vary substantially among different species based on size and shell morphology. The species studied here, Cuvierina atlantica, uses a unique overlap-and-fling maneuver at the end of each half stroke and pitches its large, elongated shell by approximately 20° while swimming. In contrast, the much smaller, coiled shell thecosomes L. helicina (Chang and Yen, 2012; Murphy et al., 2016) and L. helicina antarctica (Adhikari et al., 2016) use a modified version of the clap-and-fling maneuver only at the end of the power stroke and flap their wings against the shell at the end of the recovery stroke. In addition, these thecosomes pitch their shells to a much greater degree, by up to 60° in L. helicina and up to 110° in L. helicina antarctica. These coiled shells possess much less rotational drag and moment of inertia in comparison to the elongated shell of C. atlantica, which retards such a large degree of pitching. In addition, the different Reynolds number regimes in which the tiny coiled shell species and C. atlantica operate could contribute to their different swimming kinematics. The coiled shell species generally operate in a highly viscous regime at Reynolds numbers less than 100 whereas C. atlantica, with its elongated shell, operates at a Reynolds number an order of magnitude higher (Re=100-600). The relative importance of inertial and viscous forces may have thus led this species to adopt a more streamlined shell in order to reduce the pressure drag, which would be important at this larger Re. Finally, though it would be expected that the larger species would have a lower wingbeat frequency, comparing the wingbeat frequency of C. atlantica with the tiny coiled shell species is difficult because of ambient water temperature (and thus viscosity) differences. Cuvierina atlantica lives at a water temperature of ~21° C (which has a viscosity of  $1.05 \times 10^{-6}$  m<sup>2</sup> s<sup>-1</sup>) and beats its wings at ~5 Hz. In contrast, *L. helicina* lives at ~12-16°C and has a wingbeat frequency of 5-10 Hz, and L. helicina antarctica lives at  $\sim 0^{\circ}$ C (which has a higher viscosity of 1.83×10<sup>-6</sup> m<sup>2</sup> s<sup>-1</sup>) and has a lower wingbeat frequency of 2-3 Hz (Chang and Yen, 2012; Adhikari et al., 2016; Murphy et al., 2016). The higher seawater viscosity at colder temperatures thus corresponds to lower wingbeat frequencies, though temperatureinduced differences in metabolism may also play a role here (Pétavy et al., 1997).

The swimming of the thecosome species studied here also bears some similarity to that of the shell-less gymnosomes C. limacina (Satterlie et al., 1985; Szymik and Satterlie, 2011) and C. antarctica (Borrell et al., 2005). Cuvierina atlantica and these gymnosomes have a similar elongated shape, have approximately the same body length, and flap their wings in similar, nearly horizontal stroke planes. However, compared to C. atlantica, gymnosomes have relatively short, low aspect ratio wings, and this difference in wing morphology affects their ability to perform a version of the overlap-and-fling maneuver. During slow swimming, the wingtips of *C. limacina* approach but do not touch each other. However, during fast swimming, it appears that C. limacina may perform a version of the overlap-and-fling maneuver at the end of the downstroke as the wings fold over each other close to the body (Szymik and Satterlie, 2011). Because the wings are shorter, the void between them is compressed in comparison to the cylindrical void formed by the wings of C. atlantica. However, similar to C. atlantica, gymnosome wings unfold in an upward-opening cone, presumably in order to gain lift from a leading edge vortex. Another difference between C. atlantica and gymnosomes is the wingbeat frequency. Gymnosomes living at an ambient seawater temperature of 0°C flap their wings at ~1-3 Hz. This lower beat frequency may be due to the higher viscosity of colder seawater, metabolic and physiologic constraints, and the lack of a heavy calcareous shell. The lack of a shell in gymnosomes would result in a smaller wing loading and thus allow a smaller wingbeat frequency for propulsion (Pétavy et al., 1997). Further, the low aspect ratio wings of gymnosomes are not efficient for long periods of swimming but are well suited for generating high forces necessary for maneuvering. Correspondingly, gymnosomes swim slowly most of the time (at Re<100) but swim very fast (Re>1000) for short periods of time when escaping or hunting. In contrast, C. atlantica has a larger wing aspect ratio and is thus well suited to swim the long distances necessary for diel vertical migration while benefiting from the double overlap-and-fling which aids in generating the forces needed to carry the heavy shell.

398

399

400

401

402

403

404

405

406

407

408

409

410

411

412

413

414

415

416

417

418

419

420

421

422

423

424

425

426

427

428

429

430

431

It is also worth noting that the cylindrical overlap-and-fling mechanism observed here employs both suction- and jet-based propulsion mechanisms. Specifically, *C. atlantica* manipulates its wing positions to generate a low pressure suction region on the upper wing surface in the fling phase and to generate thrust by pushing the flow downward during the overlap phase. It is likely that suction dominates in thrust generation because, as shown in Figure 4d, the animal accelerates during the fling phase and decelerates during the overlap phase. Many other efficient aquatic swimmers such as jellyfish and lampreys similarly rely on suction for thrust generation (Gemmell et al., 2015). Indeed, the kinematics of the overlap-

432 and-fling mechanism bear some similarity to the bell kinematics of jellyfish medusae (Dabiri et al., 2005; Gemmell et al., 2018) and jellyfish-inspired robots (Nawroth et al., 2012; 433 Ristroph and Childress, 2014; Ren et al., 2019). Finally, the swimming mechanisms of 434 marine molluscs in general (Borrell et al., 2005; Szymik and Satterlie, 2011; Chang and Yen, 435 2012; Adhikari et al., 2016; Murphy et al., 2016; Zhou and Mittal, 2017; Zhou and Mittal, 436 2018) and the cylindrical overlap-and-fling mechanism observed here in particular may serve 437 as bioinspiration for new soft robotic aquatic vehicles propelled by highly flexible propulsors 438 capable of taking advantage of this and other novel lift generation techniques. 439 440

Acknowledgements 442 The authors gratefully acknowledge Leocadio Blanco-Bercial for assistance in collecting the 443 pteropods, Joseph Bello for assistance in conducting experiments, and Paola Rossi Bruttini 444 for assistance with digitization. 445 446 447 **Competing interests** The authors declare no competing or financial interests. 448 449 450 **Author contributions** F.K., D.W.M., and A.E.M conceived and designed the experiment. F.K. and D.W.M carried 451 out experimental work and data analysis. A.E.M. procured and identified the animals. F.K., 452 D.W.M., and A.E.M. wrote the manuscript. All authors approved the final manuscript. 453 454 **Funding** 455 Funding was provided by a National Science Foundation CAREER grant to D.W.M. (CBET 456 #1846925), a grant from the National Academies of Science Keck Futures Initiative (NAKFI) 457 to A.E.M and D.W.M, a University of South Florida (USF) New Researcher Grant to 458 459 D.W.M, a USF Nexus Grant to D.W.M., and a Bermuda Institute of Ocean Sciences Grant in Aid to D.W.M. 460 461 462 **Supplementary movies** Movie 1. Visualization of swimming C. atlantica taken from two orthogonal high speed 463 cameras. Movies acquired at 600 frames per second and played back at 25 frames per 464 second. 465 Movie 2. Flow measurements of *C. atlantica* swimming. Vectors indicate flow direction 466 and magnitude, and color contours represent vorticity. Recorded at 1400 frames per second 467 and played back at 25 frames per second. 468 469

471 References

- 473 **Abdel-Aziz, Y. I. and Karara, H. M.** (1971). Direct linear transformation from comparator 474 coordinates into object space coordinates in close-range photogrammetry. In *In Proceedings of* 475 *the ASP/UI Symposium on Close-Range Photogrammetry*, pp. 1–18.
- Adhikari, D., Webster, D. R. and Yen, J. (2016). Portable tomographic PIV measurements of swimming shelled Antarctic pteropods. *Exp. Fluids* **57**, 1–17.
- Bomphrey, R. J., Nakata, T., Phillips, N. and Walker, S. M. (2017). Smart wing rotation and trailing-edge vortices enable high frequency mosquito flight. *Nature* **544**, 92–95.
- Borrell, B. J., Goldbogen, J. a and Dudley, R. (2005). Aquatic wing flapping at low Reynolds
  numbers: swimming kinematics of the Antarctic pteropod, *Clione antarctica*. *J. Exp. Biol.* 208,
  2939–2949.
- 483 Chang, Y. and Yen, J. (2012). Swimming in the Intermediate Reynolds Range: Kinematics of the Pteropod Limacina helicina. *Integr. Comp. Biol.* **52**, 597–615.
- 485 **Cheng, X. and Sun, M.** (2017). Aerodynamic forces and flows of the full and partial clap-fling motions in insects. *PeerJ* **2017**,.
- 487 Cheng, X. and Sun, M. (2018). Very small insects use novel wing flapping and drag principle to generate the weight-supporting vertical force. *J. Fluid Mech.* 855, 646–670.
- Colin, S. P., Costello, J. H., Dabiri, J. O., Villanueva, A., Blottman, J. B., Gemmell, B. J. and
  Priya, S. (2012). Biomimetic and Live Medusae Reveal the Mechanistic Advantages of a
  Flexible Bell Margin. *PLoS One* 7,.
- 492 **Combes, S. A. and Daniel, T. L.** (2003a). Flexural stiffness in insect wings I. Scaling and the influence of wing venation. *J. Exp. Biol.* **206**, 2979–2987.
- 494 Combes, S. A. and Daniel, T. L. (2003b). Flexural stiffness in insect wings. II. Spatial distribution and dynamic wing bending. *J. Exp. Biol.* **206**, 2989–2997.
- 496 **Cooter, R. J. and Baker, P. S.** (1977). Weis-Fogh clap and fling mechanism in Locusta. *Nature* **269**, 497 53–54.
- 498 **Dabiri, J. O., Colin, S. P., Costello, J. H. and Gharib, M.** (2005). Flow patterns generated by oblate medusan jellyfish: Field measurements and laboratory analyses. *J. Exp. Biol.* **208**, 1257–1265.
- Dickinson, M. H. (1996). Unsteady Mechanisms of Force Generation in Aquatic and Aerial
  Locomotion. Am. Zool. 36, 537–554.
- 502 **Dickinson, M. H., Lehmann, F. O. and Sane, S.** (1999). Wing Rotation and the Aerodynamic Basis of Insect Flight. *Science* (80-.). **284**, 1954–1960.
- Ellington, C. P. (1984). The aerodynamics of flapping animal flight. Am. Zool. 24, 95–105.
- Gemmell, B. J., Jiang, H. and Buskey, E. J. (2014). A new approach to micro-scale particle image
  velocimetry (PIV) for quantifying flows around free-swimming zooplankton. *J. Plankton Res.* 36, 1396–1401.
- Gemmell, B. J., Colin, S. P., Costello, J. H. and Dabiri, J. O. (2015). Suction-based propulsion as a basis for efficient animal swimming. *Nat. Commun.* **6**, 8790.
- Gemmell, B. J., Colin, S. P. and Costello, J. H. (2018). Widespread utilization of passive energy
  recapture in swimming medusae. *J. Exp. Biol.* 221,.
- Hedrick, T. L. (2008). Software techniques for two- and three-dimensional kinematic measurements
  of biological and biomimetic systems. *Bioinspir. Biomim.* 3, 034001.

- Janssen, A. W. and Peijnenburg, K. T. C. A. (2017). An overview of the fossil record of Pteropoda (Mollusca, Gastropoda, Heterobranchia). *Cainozoic Res.* 17, 3–10.
- Karakas, F., D'Oliveira, D., Maas, A. E. and Murphy, D. W. (2018). Using a shell as a wing: pairing of dissimilar appendages in atlantiid heteropod swimming. *J. Exp. Biol.* **221**, jeb192062.
- Kodali, D., Medina, C., Kang, C. K. and Aono, H. (2017). Effects of spanwise flexibility on the performance of flapping flyers in forward flight. *J. R. Soc. Interface* 14,.
- Kolomenskiy, D., Moffatt, H. K., Farge, M. and Schneider, K. (2011). The Lighthill-Weis-Fogh clap-fling-sweep mechanism revisited. *J. Fluid Mech.* **676**, 572–606.
- Koutsiaris, A. G. (2012). Digital micro PIV (μPIV) and velocity profiles in vitro and in vivo. In In
  The particle image velocimetry-characteristics, limits and possible applications, .
- Lehmann, F. O., Sane, S. P. and Dickinson, M. (2005). The aerodynamic effects of wing-wing interaction in flapping insect wings. *J. Exp. Biol.* **208**, 3075–3092.
- Lighthill, M. J. (1973). On the Weis-Fogh mechanism of lift generation. J. Fluid Mech. 60, 1–17.
- Lucas, K. N., Johnson, N., Beaulieu, W. T., Cathcart, E., Tirrell, G., Colin, S. P., Gemmell, B. J.,
  Dabiri, J. O. and Costello, J. H. (2014). Bending rules for animal propulsion. *Nat. Commun.* 5,
  1–7.
- Marden, J. H. (1987). Maximum lift production during takeoff in flying animals. J. Exp. Biol. Vol.
  130, 235–258.
- 532 **Maxworthy, T.** (1979). Experiments on the Weis-Fogh mechanism of lift generation by insects in hovering flight. Part 1. Dynamics of the 'fling.' *J. Fluid Mech.* **93**, 47–63.
- Miller, L. A. and Peskin, C. S. (2005). A computational fluid dynamics of 'clap and fling' in the smallest insects. *J. Exp. Biol.* **208**, 195–212.
- Miller, L. A. and Peskin, C. S. (2009). Flexible clap and fling in tiny insect flight. *J. Exp. Biol.* 212, 3076–3090.
- 538 **Murphy, D. W., Adhikari, D., Webster, D. R. and Yen, J.** (2016). Underwater flight by the planktonic sea butterfly. *J. Exp. Biol.* **219**, 535–543.
- Nawroth, J. C., Lee, H., Feinberg, A. W., Ripplinger, C. M., McCain, M. L., Grosberg, A.,
  Dabiri, J. O. and Parker, K. K. (2012). A tissue-engineered jellyfish with biomimetic
  propulsion. *Nat. Biotechnol.* 30, 792–797.
- Peijnenburg, K. T. C. A., Janssen, A. W., Wall-Palmer, D., Goetze, E., Burridge, A. K., Maas, A. E., Todd, J. and Marlétaz, F. Early Cretaceous origin of pteropods suggests their resilience to ocean acidification. (Manuscript submitted for publication).
- Percin, M., Van Oudheusden, B. and Remes, B. (2017). Flow structures around a flapping-wing micro air vehicle performing a clap-and-peel motion. *AIAA J.* **55**, 1251–1264.
- Pétavy, G., Morin, J. P., Moreteau, B. and David, J. R. (1997). Growth temperature and
  phenotypic plasticity in two Drosophila sibling species: Probable adaptive changes in flight
  capacities. *J. Evol. Biol.* 10, 875–887.
- Ren, Z., Hu, W., Dong, X. and Sitti, M. (2019). Multi-functional soft-bodied jellyfish-like
  swimming. *Nat. Commun.* 10,.
- Ristroph, L. and Childress, S. (2014). Stable hovering of a jellyfish-like flying machine. J. R. Soc.
  Interface 11, 20130992.
- Sane, S. P. (2016). Neurobiology and biomechanics of flight in miniature insects. *Curr. Opin. Neurobiol.* 41, 158–166.

Santhanakrishnan, A., Robinson, A. K., Jones, S., Low, A. A., Gadi, S., Hedrick, T. L. and
 Miller, L. A. (2014). Clap and fling mechanism with interacting porous wings in tiny insect

flight. J. Exp. Biol. 217, 3898–3909.

587

- Satterlie, R. A., Labarbera, M. and Spencer, A. N. (1985). Swimming in the Pteropod Mollusk,
  Clione-Limacina .1. Behavior and Morphology. J. Exp. Biol. 116, 189–204.
- 562 **Srygley, R. B. and Thomas, A. L. R.** (2002). Unconventional lift-generating mechanisms in free-flying butterflies. *Nature* **420**, 660–664.
- 564 Szymik, B. G. and Satterlie, R. a (2011). Changes in wingstroke kinematics associated with a change in swimming speed in a pteropod mollusk, *Clione limacina*. *J. Exp. Biol.* **214**, 3935–47.
- 566 **Szymik, B. G. and Satterlie, R. A.** (2017). Circulation of hemocoelic fluid during slow and fast swimming in the pteropod mollusc Clione limacina. *Invertebr. Biol.* **136**, 290–300.
- Thabet, A. A., Maas, A. E., Lawson, G. L. and Tarrant, A. M. (2015). Life cycle and early
  development of the thecosomatous pteropod Limacina retroversa in the Gulf of Maine, including
  the effect of elevated CO2 levels. *Mar. Biol.* 162, 2235–2249.
- Vanella, M., Fitzgerald, T., Preidikman, S., Balaras, E. and Balachandran, B. (2009). Influence
  of flexibility on the aerodynamic performance of a hovering wing. *J. Exp. Biol.* 212, 95–105.
- Vogel, S. (1966). Flight in Drosophila: I. Flight Performance of Tethered Flies. J. Exp. Biol. 44, 567–
  578.
- Weis-Fogh, T. (1973). Quick estimates of flight fitness in hovering animals, including novel mechanisms for lift production. *J. Exp. Biol.* **59**, 169–230.
- Wong, J. G. and Rival, D. E. (2017). Rapid manoeuvring with spanwise-flexible wings. *J. Fluids* Struct. 75, 1–8.
- 579 Wootton, R. J. (1981). Support and deformability in insect wings. J. Zool. 193, 447–468.
- 580 Wootton, R. J. (1990). The Mechanical Design of Insect Wings. Sci. Am. 263, 114–120.
- Wormuth, J. H. (1981). Vertical distributions and diel migrations of Euthecosomata in the northwest
  Sargasso Sea. Deep Sea Res. Part A, Oceanogr. Res. Pap. 28, 1493–1515.
- **Zhou, Z. and Mittal, R.** (2017). Swimming without a Spine: Computational Modeling and Analysis of the Swimming Hydrodynamics of the Spanish Dancer. *Bioinspir. Biomim.* **13**, p.015001.
- **Zhou, Z. and Mittal, R.** (2018). Swimming performance and unique wake topology of the sea hare (*Aplysia*). *Phys. Rev. Fluids* 3,.

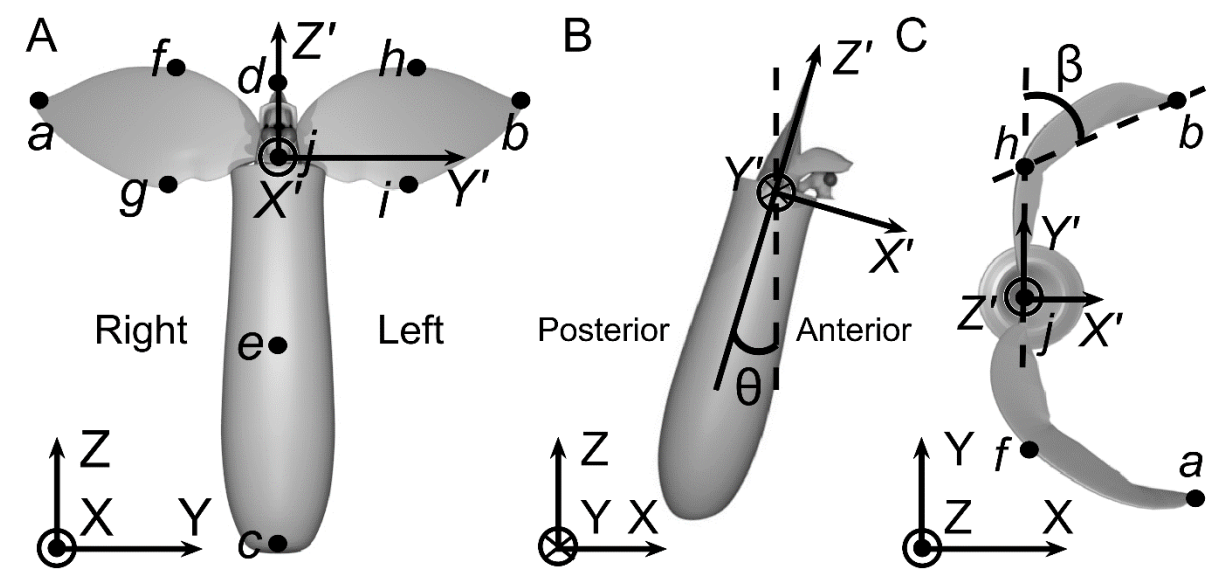


**Fig. 1.** Cuvierina atlantica morphology and coordinate systems. (A) Front view, (B) side view, and (C) top view showing the locations of the tracked points (a-j), the definition of the body angle  $\theta$ , the definition of the wing bending angle  $\beta$  for the left wing, the global coordinate system (XYZ), and the body-centered (X'Y'Z') coordinate system. The origin of the X'Y'Z' coordinate system is located at point j. The wing bending angle for the right wing is similarly calculated using points f and a.

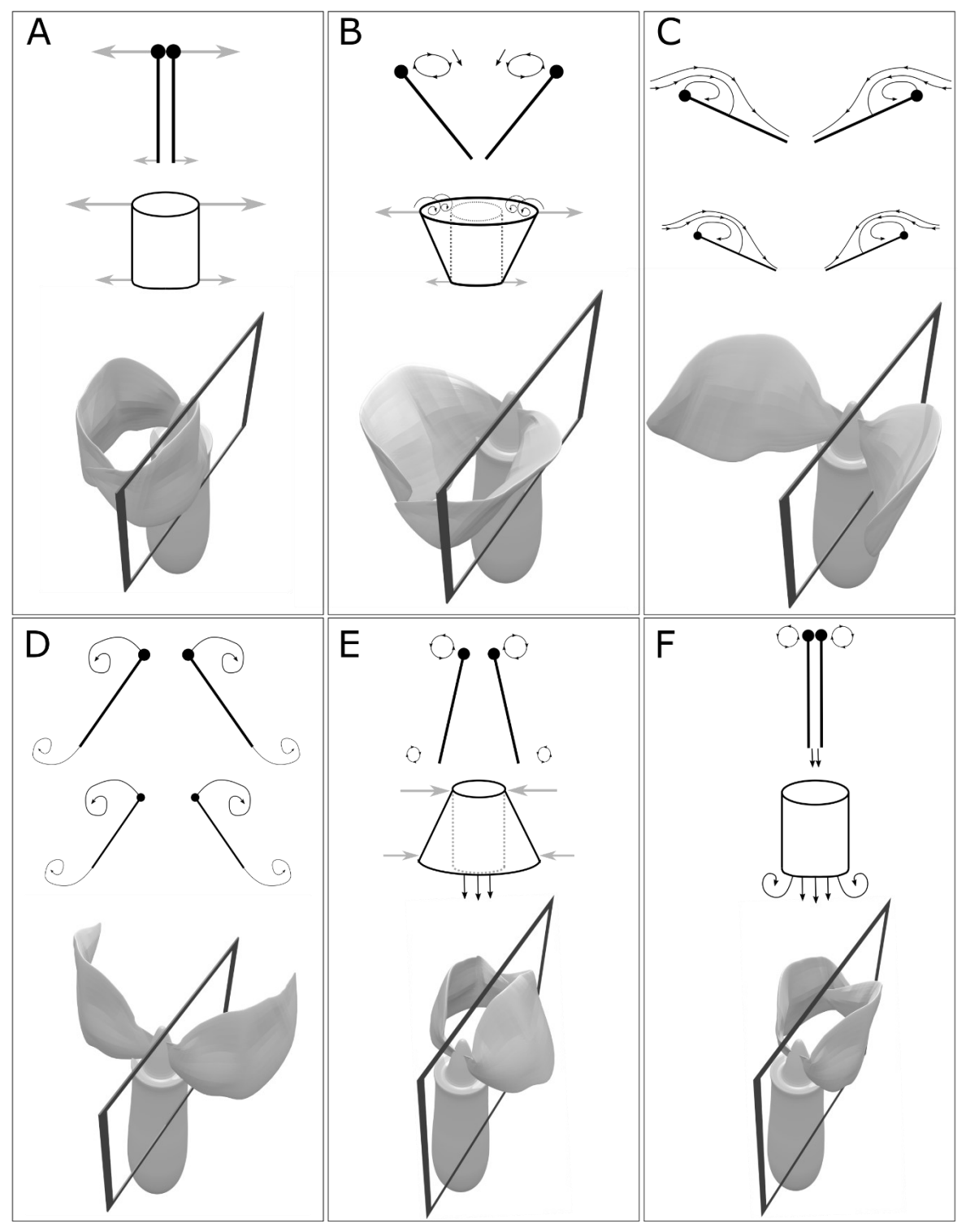
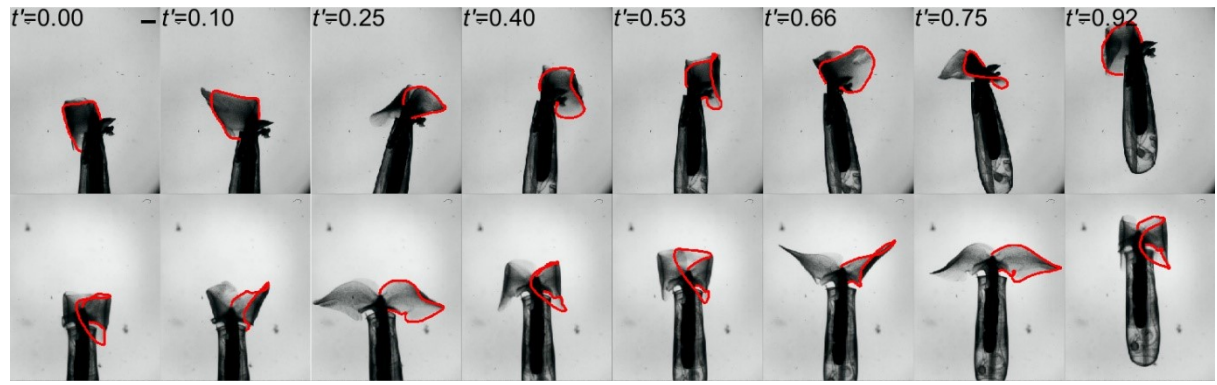
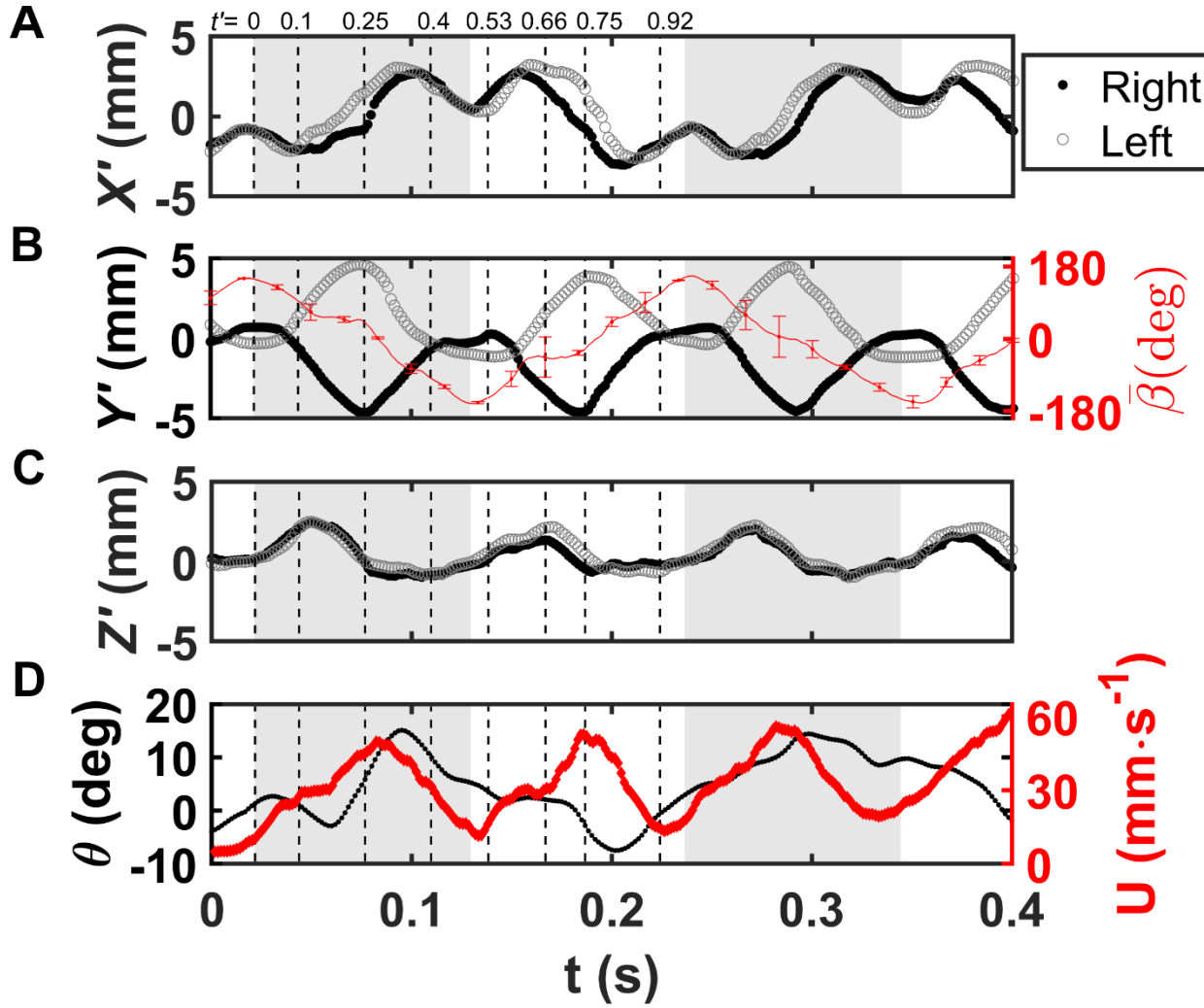


Fig. 2. Schematic of model pteropod wings performing the cylindrical overlap-and-fling maneuver as compared to planar wings performing the clap-and-fling maneuver. (A-C) Illustration of flow into opening cylinder during the fling. Wing orientation during fling at (A) t'=0, (B) t'=0.1, and (C) t'=0.25. (D-F) Illustration of flow exiting cylinder during the overlap. Wing orientation at (D) t'=0.35, (E) t'=0.4, and (F) t'=0.53. Within each panel, the top, middle, and bottom figures represents the traditional clap-and-fling maneuver, the overlap-and-fling maneuver, and a 3D rendering of the wing positions of C. atlantica performing the overlap-and-fling maneuver, respectively. The rectangle in each 3D rendering represents the location of the flow measurement focal plane relative to the animal in Fig. 5.



**Fig. 3. Pteropod wing stroke.** Sequence of synchronized images acquired from two orthogonal perspectives illustrating one stroke cycle. The top row views the animal from its right side, and the bottom row views the animal from its posterior. The variable t' is time normalized by the stroke period (200 ms). The scale bar represents 1 mm. The right wing of the animal is outlined in both views.



**Fig. 4. Pteropod wing and body kinematics.** Wing and body kinematics of *C. atlantica* over slightly less than two stroke cycles. (A-C) Right and left wingtip trajectories in the bodycentered coordinate system. (B) mean and standard deviation of wing bending angle  $\bar{\beta}$  averaged between the left and right wings. (D) Body angle  $\theta$  and swimming speed U. The power stroke is shaded gray. Dashed vertical lines correspond to non-dimensionalized times shown in Fig. 3.

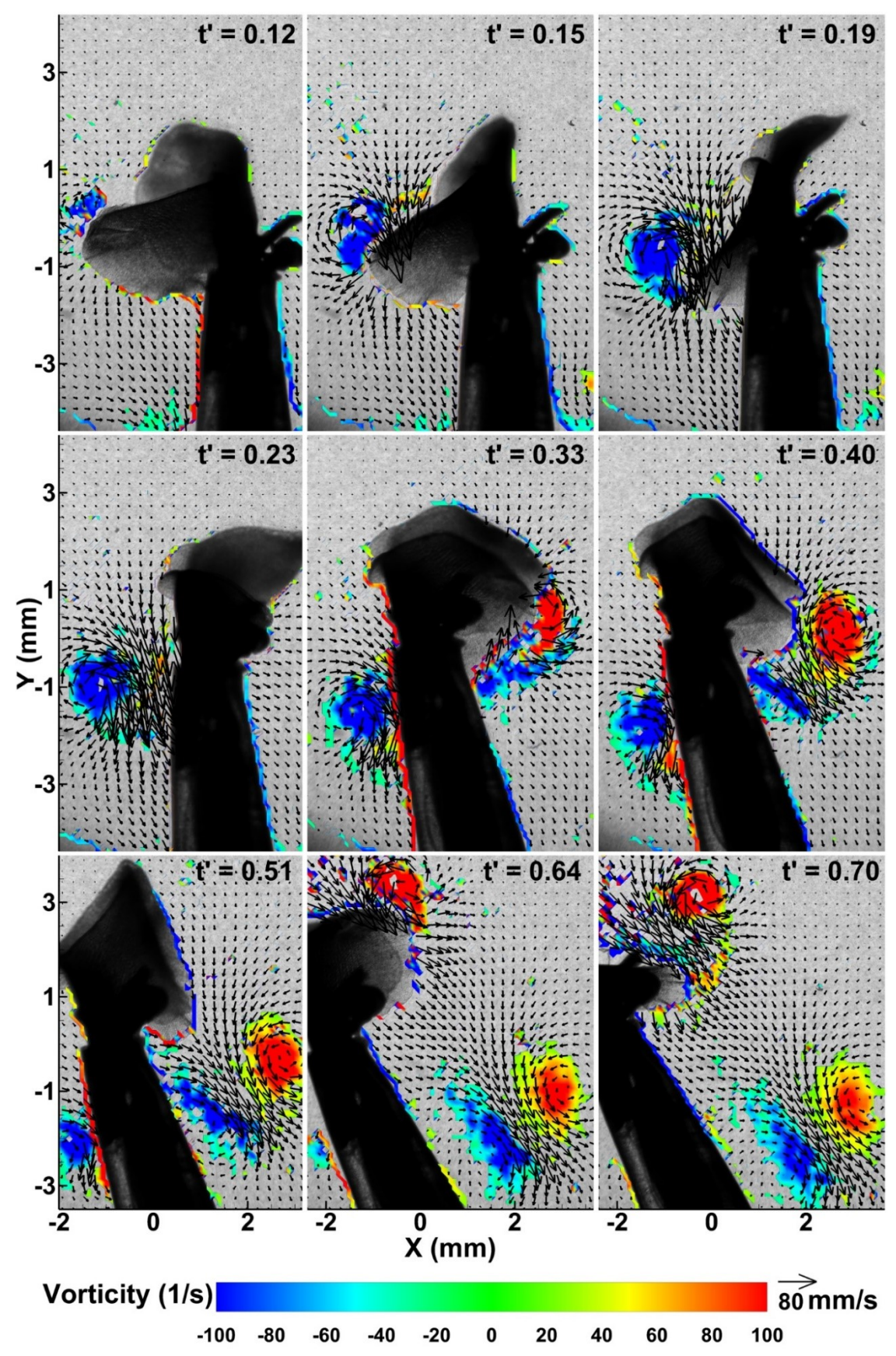


**Fig. 5. Flow field.** Time sequence of the velocity and vorticity fields generated as *C. atlantica* performs a cylindrical overlap-and-fling maneuver. Color contours represent the z-component of vorticity, and vectors indicate flow direction and magnitude. The measurement

plane intersects the animal as shown in Fig. 2. The variable t' is time normalized by the stroke period (200 ms).